On the Photoabsorption Spectroscopy of Water

Badry D. Bursulaya,† Jonggu Jeon, Chia-Ning Yang, and Hyung J. Kim*

Department of Chemistry, Carnegie Mellon University, 4400 Fifth Avenue, Pittsburgh, Pennsylvania 15213-2683

Received: July 26, 1999; In Final Form: October 12, 1999

The first photoabsorption band of water around 8 eV is studied with the molecular dynamics computer simulation technique under ambient and supercritical conditions. By employment of the polarizable TAB/10D potential model (Bursulaya, B. D.; Jeon, J.; Zichi, D. A.; Kim, H. J. *J. Chem. Phys.* **1997**, *108*, 3286), the electronic structure variations of the ground and low-lying excited states of water with solvation are explicitly accounted for via the truncated adiabatic basis-set representation. Compared with the $\tilde{X}^1A_1 \rightarrow \tilde{A}^1B_1$ transition in vacuum, the absorption spectrum tends to be blue-shifted and broadened in solution, consonant with experiments. It is found that both the solvation and Rydbergization destabilizations of the first excited states of individual water molecules, compared with their respective ground states, contribute to the blue shift, while the line broadening arises from the inhomogeneous distribution of their solvation environments. Also there is significant electronic mixing of the excited states, induced by solvation. As a result, their dipole character varies dramatically with the fluctuating solvation environment as well as with the thermodynamic conditions, e.g., density. Its potential consequences for the Urbach tail of the spectrum observed in condensed phases are discussed. Also new insights into multiphoton ionization of water from the excited-state electronic perspective are presented.

I. Introduction

Photoabsorption spectroscopy is one of the important means to probe water excited states and its photophysical and photochemical properties.[1] As such, it has received extensive attention for quite some time.[2−12] Despite these efforts, however, the excited state electronic structure variation with solvation and its influence on, e.g., absorption line shape in the condensed phases are still not well understood. For instance, the maximum intensity line of the first photoabsorption band is blue-shifted to ∼8.2 eV in liquid water and ∼8.4 eV in ice,[2−11] compared with that of vapor near 7.4 eV.[12] This is usually attributed to the Rydbergization effect.[13] To be specific, highly Rydberg-like excited states overlap strongly with the core electronic states of neighboring water molecules, so that they become destabilized in the condensed phases through the enhanced exchange repulsion, compared with the ground state.[14] The increasing blue-shift observed for matrix-isolated water with the decreasing size of the matrix constituents appears to confirm this view.[15] However, this does not explain, e.g., larger blue shift in ice than in ambient water because the exchange repulsion is expected to be weaker in the former because of its lower density than in the latter. Considering also the well-established result that the dipole directions of the ground and first excited states of water are opposite to each other,[16] we would expect that other factors, e.g., solvation, could play a significant role as well.

Another interesting feature in photoabsorption of water is a long tail ("Urbach tail") which appears on the red edge of the lowest band in the condensed phases. Although this was not observed in reflectance experiments,[5,10] the existence of the tail is generally accepted from transmission studies.[3,4,6,8,9] There it is found that the tail is extended into the low-energy region—much more so in liquid water than in ice—even below the absorption band of vapor. Its intensity decreases nearly exponentially with diminishing photon energy. It also shifts toward longer wavelengths as the temperature rises. Several theories have been proposed to explain the origin of the tail in water, including the localized excitations,[3a,8] tail of a Gaussian absorption band,[3b] charge transfer between water molecules,[1a] and excited-state character change from Rydberg to valence-bond states with the elongation of the intramolecular O−H bond.[15] As indicated by the number of widely different models, the origin of the tail is largely unresolved and is still the object of ongoing controversy.[1]

There have been only a few theoretical studies on photoexcitation properties of liquid water. The main reason for sparsity is presumably the technical difficulty associated with the incorporation of a solvent electronic description—which allows for excitations—into the simulation algorithms. Laasonen et al. conducted a density functional simulation study to analyze the HOMO−LUMO gap of water.[17] Borgis and Staib examined the solvation effects on absorption using a four-state valence-bond description.[18] By employing the truncated adiabatic basis-set (TAB) description,[19] Kim and co-workers investigated the first absorption band of ambient water and obtained reasonable agreement with measurements, including blue shift.[20] Various ab initio calculations predict spectral blue shift also for small clusters $(H_2O)_n$ $(n = 2-6)$.[21−24]

In this paper, we extend our previous simulation study of electronic spectroscopy[20] by including the Rydbergization destabilization and present a detailed analysis of the environmental effects on spectral line shape. For comparison, we also analyze the Stark effect on the ground and first excited states of an isolated water molecule using the ab initio quantum chemistry methods. Our results indicate that the dipole moment

* Author to whom correspondence should be addressed.
† Present address: Department of Molecular Biology, The Scripps Research Institute, La Jolla, CA 92037.

10.1021/jp992582g CCC: $19.00
Published on Web 12/03/1999

of the excited states relevant for the first absorption band varies significantly with the photon energy. Also their electronic character is strongly modulated by the thermodynamic conditions. For instance, the average dipole direction of the first excited states of water molecules varies with density; it is parallel to the ground-state dipole in ambient water, whereas it is antiparallel under low-density supercritical conditions. This is due to the solvation-dependent electronic mixing of the excited states. Its consequences for the spectral line shape, in particular, Urbach tail, and implications for multiphoton ionization[25,26] are considered. Also as an experimental probe of the excited-state electronic structure variations of water with solvation, Stark-effect spectroscopy[27] is suggested.

The outline of this paper is as follows. In section II we briefly review the theoretical formulation for the solvent electronic description based on TAB. Ab initio results on the Stark effect for an isolated water molecule are presented in section III. In section IV, the simulation results for the photoabsorption spectra of water are analyzed. A novel interpretation of its Urbach tail and a new insight into multiphoton ionization of water are presented. The concluding remarks are offered in section V.

II. TAB Theory

We begin with a brief summary of the TAB formulation for the solvent electronic description of ref 19. We repeat only the formulas essential to establishing our notation and to analyzing photoabsorption. For details, the reader is referred to ref 19.

In the TAB approach, the electronic wave function ψ_n^i of molecule i ($i = 1, 2, ..., N$) in solution is expressed as a linear combination of a few multielectron wave functions ϕ_μ^i ($\mu = 0, 1, ...$) that are the eigenstates of its vacuum Hamiltonian $\hat{h}^i$

$$\psi_n^i = \sum_\mu c_{n\mu}^i \phi_\mu^i; \quad \hat{h}^i \phi_\mu^i = \epsilon_\mu^{\mathrm{vac},i} \phi_\mu^i \tag{1}$$

where n labels the single-molecule states in solution and $\epsilon_\mu^{\mathrm{vac},i}$ is the vacuum energy eigenvalue. Because of the intermolecular Coulombic interactions in solution, the state coefficients $c_{n\mu}^i$ for each i fluctuate with its surrounding solvent environment.[19] Thus, the variations of dipole moment and polarizability of i are described by a solvation-dependent mixing of ϕ_μ^i's in this theory (see section III below for its limitations). Hereafter, ϕ_μ^i's will be referred to as TAB functions (or simply basis functions).

The effective Hamiltonian $\hat{H}$ for the solvent system is given by

$$\hat{H} = \sum_i \hat{h}^i + \sum_j \sum_{i(>j)} [\hat{u}_C^{ij} + u_{LJ}^{ij}] \equiv \hat{H}_{el} + \sum_j \sum_{i(>j)} u_{LJ}^{ij} \tag{2}$$

where $\hat{u}_C^{ij}$ and u_{LJ}^{ij} denote respectively the Coulombic and Lennard-Jones interactions between molecules i and j. For simplicity, we have assumed in eq 2 that u_{LJ}^{ij} is independent of the electronic states of the interacting pair. In a point-dipole approximation for the solvent charge distribution,[28] $\hat{u}_C^{ij}$ is given by

$$\hat{u}_C^{ij} = \hat{p}^i \cdot \boldsymbol{T}_{ij} \cdot \hat{p}^j; \quad \boldsymbol{T}_{ij} = \nabla_i \nabla_j \frac{1}{|\vec{r}_i - \vec{r}_j|} \quad (i \neq j) \tag{3}$$

where $\hat{p}^i$ is the electric dipole operator for i, $\vec{r}_i$ is its position vector, and $\boldsymbol{T}_{ij}$ is the dipole tensor between i and j. In the self-consistent-field (SCF) approximation, the ground-state wave function Ψ_{SCF} and electronic potential energy U of the entire solvent system are

$$|\Psi_{SCF}\rangle = \prod_{i=1}^{N} |\psi_0^i\rangle; \qquad \epsilon_0 = \sum_i \epsilon_0^i$$

$$E_{SCF}^G = \langle \Psi_{SCF} | \hat{H}_{el} | \Psi_{SCF} \rangle = \epsilon_0 - \sum_j \sum_{i(>j)} \vec{\mu}^i \cdot \boldsymbol{T}_{ij} \cdot \vec{\mu}^j$$

$$U = \langle \Psi_{SCF} | \hat{H} | \Psi_{SCF} \rangle = E_{SCF}^G + \sum_j \sum_{i(>j)} u_{LJ}^{ij} \tag{4}$$

where the single-molecule wave function and energy, ψ_n^i and ϵ_n^i ($n = 0, 1, ...$), satisfy a set of "Fock" equations

$$\hat{f}^i |\psi_n^i\rangle = [\hat{h}^i + \hat{u}_{1M}^i] |\psi_n^i\rangle = \epsilon_n^i |\psi_n^i\rangle;$$
$$\hat{u}_{1M}^i \equiv \sum_{j(\neq i)} \vec{\mu}^j \cdot \boldsymbol{T}_{ji} \cdot \hat{p}^i; \quad \vec{\mu}^i = \langle \psi_0^i | \hat{p}^i | \psi_0^i \rangle \tag{5}$$

and $\vec{\mu}^i$ is the ground-state dipole expectation value of i.

To study electronic spectroscopy, we consider Ψ_a^i

$$|\Psi_a^i\rangle = [\prod_{j(\neq i)} |\psi_0^j\rangle] |\psi_a^i\rangle \quad (a \neq 0) \tag{6}$$

where molecule i is excited from its ground state to level a. Thus, Ψ_a^i's describe the situation where only one water molecule is electronically excited while the rest of the molecules are in their respective ground states. As such, they represent excitations localized to a single molecule with the complete neglect of electronic relaxation. Hereafter, Ψ_a^i's will be referred to as one-molecule excited states (1MES). The energy differences between the SCF ground state and 1MES are

$$\Delta E_a^i = \langle \Psi_a^i | \hat{H} | \Psi_a^i \rangle - \langle \Psi_{SCF} | \hat{H} | \Psi_{SCF} \rangle = E_{SCF}^G + \epsilon_a^i - \epsilon_0^i \tag{7}$$

Analogous to Brillouin's theorem in gas-phase electronic structure theory,[29] Ψ_a^i's are not directly coupled to Ψ_{SCF}.[19] Thus, we can perform configuration interaction calculations among 1MES. Hereafter, this will be referred to as 1MCI. This provides a size-consistent method for the excited states, which takes into account a certain electronic relaxation effect, i.e., exciton delocalization, accompanying electronic transitions. It involves the diagonalization of a CI matrix

$$\langle \Psi_a^i | \hat{H}_{el} | \Psi_b^j \rangle = (E_{SCF}^G + \epsilon_a^i - \epsilon_0^i)\delta_{ab}\delta_{ij} + \vec{p}_{a0}^i \cdot \boldsymbol{T}_{ij} \cdot \vec{p}_{0b}^j (1 - \delta_{ij})$$
$$(a, b \neq 0) \tag{8}$$

where $\vec{p}_{a0}^i$ is the transition dipole moment between ψ_a^i and ψ_0^i.

III. Stark Effect on Water Electronic Structure

Before we embark on our simulation study, we first investigate the electronic structure of an isolated water molecule subject to a uniform electric field with the CASSCF (complete active space self-consistent field) quantum chemistry method. The reason for this is 2-fold, i.e., to gain insight into (1) the effects of the electric field arising from the solution environment on electronic structure and (2) the limitations of the TAB description [section II] employed in the simulations. We used the augmented cc-pVDZ basis of Dunning et al. in the ab initio calculations; this is of double-zeta quality extended by the addition of polarization and diffuse functions for each atom including hydrogen.[30] To include the effects of the Rydberg states, we also added the Rydberg basis of Dunning and Hay[31] to oxygen. The resulting basis (aug-cc-pVDZ + DH−Rydberg)[32] yields 53 AOs (atomic orbitals) for water. The CASSCF

TABLE 1: CASSCF Results for an Isolated Water Molecule

A. Vacuum Energy Gap[a]

state	CASSCF	expt[b]
$\tilde{A}^1B_1$	7.58	7.3−7.49
$\tilde{B}^1A_1$	9.80	9.69−9.73
$\tilde{C}^1B_1$	10.45	9.99−10.10
$\tilde{D}^1A_1$	10.52	10.14−10.17
$^1B_2$	11.33	11.4

B. Dipole Matrix Elements[c]

state	$\tilde{X}^1A_1$	$\tilde{A}^1B_1$	$\tilde{B}^1A_1$	$\tilde{C}^1B_1$	$\tilde{D}^1A_1$	$^1B_2$
$\tilde{X}^1A_1$	$1.84\hat{z}$					
$\tilde{A}^1B_1$	$-1.33\hat{x}$	$-1.66\hat{z}$				
$\tilde{B}^1A_1$	$1.69\hat{z}$	$-0.22\hat{x}$	$-0.98\hat{z}$			
$\tilde{C}^1B_1$	$-0.32\hat{x}$	$5.36\hat{z}$	$0.01\hat{x}$	$5.78\hat{z}$		
$\tilde{D}^1A_1$	$0.99\hat{z}$	$4.87\hat{x}$	$1.88\hat{z}$	$0.848\hat{x}$	$-0.380\hat{z}$	
$^1B_2$	$-0.85\hat{y}$	0	$-7.48\hat{y}$	0	$4.13\hat{y}$	$-1.62\hat{z}$

[a] Units: eV. [b] Reference 12. [c] Units: D.

TABLE 2: CASSCF Results for the Ground and First B_1 Excited States in the Presence of an External Electric Field

field strength (V/Å)	dipole moment (D)		energy (hartree)		excitation energy (eV)
	$\tilde{X}^1A_1^\epsilon$	$\tilde{A}^1B_1^\epsilon$	$\tilde{X}^1A_1^\epsilon$	$\tilde{A}^1B_1^\epsilon$	
0.00	+1.837	−1.660	−76.2198	−75.9413	7.578
0.25	+1.954	−0.143	−76.2188	−75.9349	7.725
0.40	+2.022	+1.155	−76.2183	−75.9327	7.772
0.45	+2.046	+1.772	−76.2181	−75.9323	7.778
0.50	+2.070	+2.523	−76.2180	−75.9322	7.777
0.55	+2.094	+3.448	−76.2178	−75.9324	7.768
0.75	+2.186	+8.786	−76.2174	−75.9377	7.611
1.00	+2.303	+14.297	−76.2170	−75.9558	7.108
1.50	+2.537	+17.397	−76.2169	−76.0085	5.670
2.00	+2.776	+18.344	−76.2177	−76.0677	4.081

calculations were performed with 1 core and 12 active MOs (molecular orbitals) by using the GAMESS code.[33] The active space is spanned by 5 a_1, 3 b_1, 3 b_2, and 1 a_2 MOs, so that each individual state is described by about 17 000 configuration state functions. The SPC (simple point charge) geometry[34] of water with a H−O−H angle of 109.5° and an O−H bond length of 1 Å was employed for all calculations.

We begin with the electronic properties of a water molecule in the absence of an external field. The results for the ground and first five dipole-allowed singlet excited states are compiled in Table 1. The convention for the molecular coordinate system is that the positive z axis is along the C_2 symmetry axis in the direction from oxygen to the center of two hydrogen atoms, the y coordinate is in the hydrogen-to-hydrogen direction, and the x axis is perpendicular to the molecular plane. The CASSCF calculations well reproduce the experimental results for electronic energies within ∼0.5 eV. They also correctly capture the dipole direction of the $\tilde{A}^1B_1$ state, which is opposite to that of the $\tilde{X}^1A_1$ state.[16] By contrast, the dipole moment of the $\tilde{C}^1B_1$ state is parallel to that of the ground state. The transition dipole moment between the two $^1B_1$ states is quite large and is in the z direction.

The ab initio results for the Stark effect on the ground and first excited states, $\tilde{X}^1A_1^\epsilon$ and $\tilde{A}^1B_1^\epsilon$, are presented in Table 2. Here the superscript ϵ is to denote explicitly the application of an external electric field ϵ_{ext} in the positive z direction. We notice several interesting features. First, the degree of dipole moment variations differs significantly between the two states (Figure 1); to be specific, $\tilde{A}^1B_1^\epsilon$ is much more polarizable than $\tilde{X}^1A_1^\epsilon$. In addition, the former shows a rather strong nonlinear electronic behavior, while the latter mainly follows linear response.

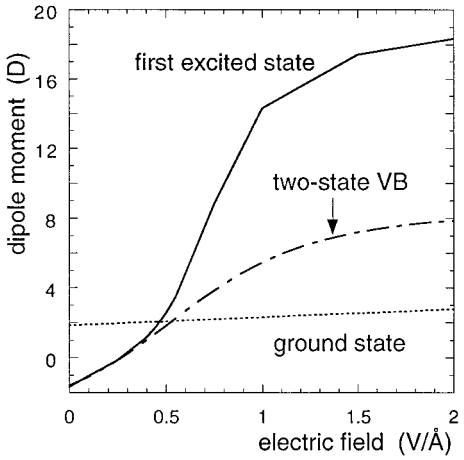

Figure 1. Dipole moments of the $\tilde{X}^1A_1^\epsilon$ (···) and $\tilde{A}^1B_1^\epsilon$ (—) states as a function of the applied field strength in vacuum. For comparison, the result of the two-state VB description for $\tilde{A}^1B_1^\epsilon$ is also shown (—·—). The ground-state dipole moment varies nearly linearly in the entire ϵ_{ext} range we have examined. By contrast, the $\tilde{A}^1B_1^\epsilon$ state shows strong nonlinear response for $0.5 \lesssim \epsilon_{ext} \lesssim 1.5$ V/Å. The two-state VB model describes the $\tilde{A}^1B_1^\epsilon$ dipole moment reasonably well up to $\epsilon_{ext} \approx 0.5$ V/Å, but it yields an underestimation for stronger ϵ_{ext}.

Another noteworthy feature is that for $0 \le \epsilon_{ext} \lesssim 0.3$ V/Å, the magnitude of the $\tilde{A}^1B_1^\epsilon$ dipole moment decreases, because of a (partial) cancellation of its permanent and induced dipole moments which are opposite in direction. For $\epsilon_{ext} \gtrsim 0.3$ V/Å, the latter becomes dominant, and as a result, the dipole moment of $\tilde{A}^1B_1^\epsilon$ changes directions and becomes parallel to that of the ground state.

To obtain a better understanding of the dipole variations of the first excited state, we consider a simple two-state model description consisting of the $\tilde{A}^1B_1$ and $\tilde{C}^1B_1$ states. For convenience, the latter two will be referred to as the valence-bond (VB) states in the rest of this section. The external field in the positive z direction affects these VB states in two ways. First, because their transition dipole moment is also along the z direction, they become electronically coupled[35] and the resulting adiabatic states are given by a mixture of the two. The lower adiabatic state defines the $\tilde{A}^1B_1^\epsilon$ state in the two-state VB description. Second, because of their opposite dipole directions, the $\tilde{A}^1B_1$ and $\tilde{C}^1B_1$ states are respectively destabilized and stabilized by ϵ_{ext}. Because their electronic coupling and energy gap respectively increases and decreases with ϵ_{ext}, their mixing increases accordingly. Therefore, the electronic polarization of $\tilde{A}^1B_1^\epsilon$ is described as a growing mixing of the VB states in the two-state model. Its dipole prediction for $\tilde{A}^1B_1^\epsilon$ is compared with the ab initio result in Figure 1. The good agreement up to $\epsilon_{ext} \approx 0.5$ V/Å indicates that the polarization of the first excited state occurs essentially via the electronic mixing of $\tilde{A}^1B_1$ and $\tilde{C}^1B_1$ in this ϵ_{ext} region. For larger ϵ_{ext}, however, the two-state model underestimates the $\tilde{A}^1B_1^\epsilon$ dipole moment. This is expected because the contributions from higher excited states are completely neglected. This alerts us that the TAB description in section II based on a few basis functions would break down, especially for the excited states, in the strong electric field regime.

Another salient feature in Table 2 is that the energy difference between $\tilde{X}^1A_1^\epsilon$ and $\tilde{A}^1B_1^\epsilon$ is a nonmonotonic function of ϵ_{ext}. To be specific, for $0 \le \epsilon_{ext} \lesssim 0.45$ V/Å, the energy gap grows with the increasing field strength. This arises from the relative destabilization of the first excited state via ϵ_{ext}, compared with the ground state. For $\epsilon_{ext} \gtrsim 0.5$ V/Å, however, the $\tilde{A}^1B_1^\epsilon$ state

TABLE 3: Parameters for the TAB/10D Model

A. Vacuum Hamiltonian[a]

diagonal elements = [0, 7.6, 9.6, 10.5, 11.0, 11.5, 14.0, 16.8, 18.0, 25.0]

B. Electric Dipole Operator[b,c]

$$\hat{p} = \begin{pmatrix} 1.85\hat{z} & -2.15\hat{x} & 1.60\hat{z} & -0.50\hat{x} & 1.20\hat{z} & -2.58\hat{y} & -3.00\hat{y} & 2.45\hat{z} & -3.00\hat{x} & 2.65\hat{z} \\ -2.15\hat{x} & -1.45\hat{z} & -0.42\hat{x} & 2.70\hat{z} & 4.20\hat{z} & 0 & 0 & 0 & 0 & 0 \\ 1.60\hat{z} & -0.42\hat{x} & -0.70\hat{z} & 0 & 1.80\hat{z} & -5.00\hat{y} & 3.45\hat{y} & 1.32\hat{z} & -2.30\hat{x} & 0 \\ -0.50\hat{x} & 2.70\hat{z} & 0 & 4.30\hat{z} & 0.84\hat{x} & 0 & 0 & 0 & 0 & 0 \\ 1.20\hat{z} & 4.20\hat{x} & 1.80\hat{z} & 0.84\hat{x} & 1.20\hat{z} & 4.00\hat{y} & 3.45\hat{y} & 1.32\hat{z} & -2.30\hat{x} & 0 \\ -2.58\hat{y} & 0 & -5.00\hat{y} & 0 & 4.00\hat{y} & -1.00\hat{z} & 0 & 0 & 0 & 0 \\ -3.00\hat{y} & 0 & 3.45\hat{y} & 0 & 3.45\hat{y} & 0 & 4.00\hat{z} & 2.35\hat{y} & 0 & 0 \\ 2.45\hat{z} & 0 & 1.32\hat{z} & 0 & 1.32\hat{z} & 0 & 2.35\hat{y} & 3.00\hat{z} & 0 & 0 \\ -3.00\hat{x} & 0 & -2.30\hat{x} & 0 & -2.30\hat{x} & 0 & 0 & 0 & -1.60\hat{z} & 0 \\ 2.65\hat{z} & 0 & 0 & 0 & 0 & 0 & 0 & 0 & 0 & -1.60\hat{z} \end{pmatrix}$$

[a] Units: eV. [b] Dipole units: D. [c] For partial charge assignment used in the actual simulations, see ref 36.

becomes highly polarized, so that it becomes more dipolar and thus better stabilized by ϵ_{ext} than $\tilde{X}^1A_1^{\epsilon}$. Therefore, the gap diminishes with growing ϵ_{ext}.

IV. Molecular Dynamics Simulation

A. Method. In the present study, we use the polarizable TAB/10D potential model with five interaction sites.[20a,b,36] The rigid SPC geometry[34] is employed for three real sites, corresponding to the oxygen and two hydrogen atoms. Two fictitious sites off the molecular plane describe the out-of-plane electronic structure variation of water. This allows for, e.g., polarizability and hyperpolarizability both in and out of the water molecular plane. Ten basis functions are employed in TAB/10D. The first six TAB functions correspond to the ground and five dipole-allowed singlet excited states of water (cf. Table 1), while the remaining four effectively represent the highly excited states that are truncated. The diagonal and overlap charge distributions of the TAB functions are represented as partial point charges centered on the five sites. In Table 3, the matrix representations of $\hat{h}^i$ and $\hat{p}^i$ for TAB/10D are presented. Their parameters are adjusted, so that they reasonably reproduce various properties of water monomer, dimer, and liquid. Thus, their values are somewhat different from the ab initio results in Table 1. For a more detailed description of the model, the reader is referred to refs 20a and 36.

The simulations were performed in the canonical ensemble of 128 water molecules using the extended system method of Nosé[37] at the following temperatures and densities: $T = 298$ K and $d = 0.997$ g cm^{-3} (AW); 673 K and 0.22 g cm^{-3} (SCW1); 673 K and 0.44 g cm^{-3} (SCW2); 673 K and 0.66 g cm^{-3} (SCW3). Periodic, truncated octahedral boundary conditions[38] were employed. All solvent bonds were constrained with the SHAKE algorithm.[39] The trajectories were integrated with a time step of 2 fs with the Verlet algorithm.[40] At each time step the single-molecule wave functions ψ_n^i were calculated by solving eq 5 iteratively; the SCF solutions were converged with a relative tolerance of 10^{-8} in total electrostatic energy.[20,36] The Coulombic interactions were computed with the Ewald method[41] with account of the self-consistency condition between the central and image molecule charges. The intermolecular forces were evaluated by differentiating U in eq 4 using the Hellmann−Feynman theorem that is exact in the SCF regime.

Equilibrium simulations were carried out with 10 ps of equilibration, followed by a 500 ps trajectory, from which averages were computed.

B. Results. The lowest photoabsorption bands of ambient and supercritical water determined via eq 7 with the neglect of electronic relaxation are displayed in Figure 2. The oscillator strength variation with the absorption energy is also ignored in the calculations. Thus, the photoabsorption spectrum in this approximation is given by the density of 1MES as a function of the energy gap ΔE_a^i. For comparison, the lowest electronic transition $\tilde{X}^1A_1 \rightarrow \tilde{A}^1B_1$ in a vacuum (cf. Table 3A) is also shown. Because of the absence of intramolecular dynamics in our model description, there is no line broadening associated with the vacuum spectrum. We, however, note that the experimental value for the full width at half-maximum (fwhm) is $\Delta_{vac} \approx 1$ eV in vacuum.[12] There are several noticeable features in Figure 2. First, there is a significant line broadening induced by solvation. This arises from the inhomogeneous distribution of differing local solvation environments for individual water molecules (see Figure 3a). Second, compared with the vacuum transition, the peak position of the first absorption band in solution is blue-shifted. Also the degree of blue shift tends to increase with the density of water although the saturation occurs at $d \approx 0.44$ g cm^{-3} (see Figure 5). The existence of an upper bound for the photon energy is directly related to the nonmonotonic behavior of the energy gap with the electric field discussed in section III.

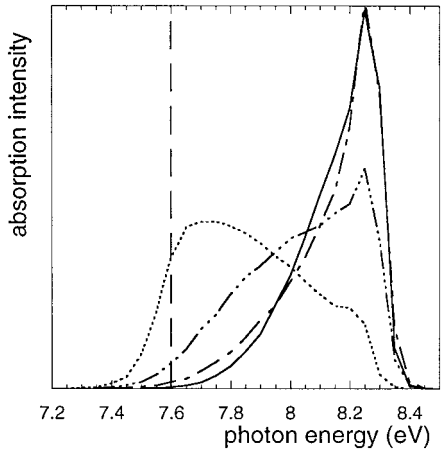

Figure 2. Distribution of 1MES energy gap ΔE_a^i: ambient (—); SCW1 (···); SCW2 (—···—); SCW3 (—·—). For comparison, the lowest vacuum transition line of TAB/10D is also shown (— —). For the entire spectrum, see ref 20a,b.

To gain insight into the effects of solvation and its fluctuations on the electronic structure and photoabsorption spectrum, we have studied the z component, ϵ_z, of the local electric field arising from the environment, evaluated at the oxygen site of the water molecules. Its probability distribution $P(\epsilon_z)$ is shown

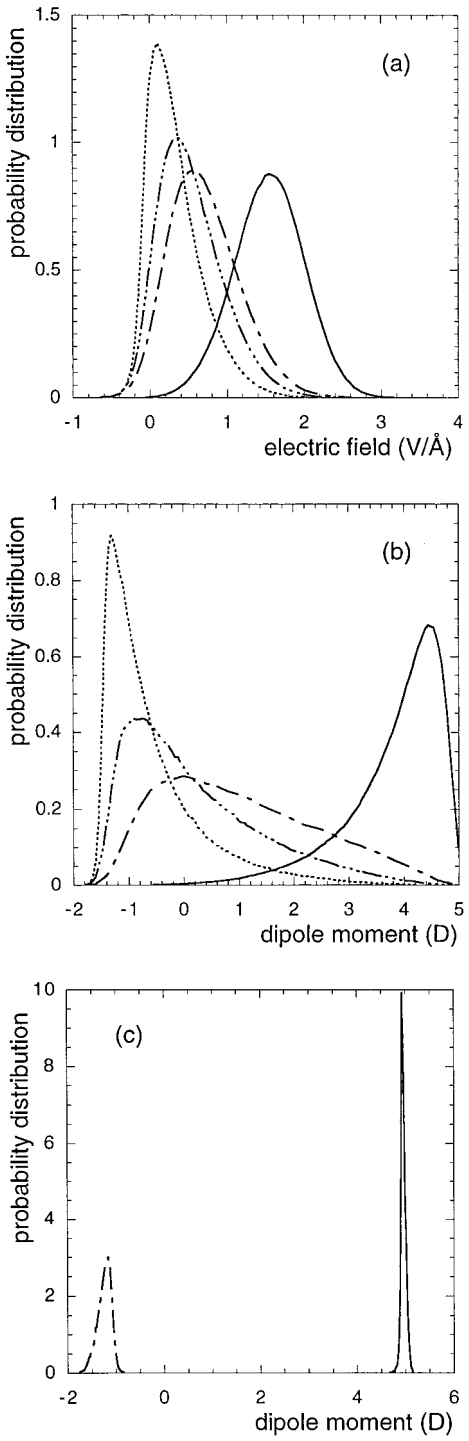

Figure 3. (a) Probability distribution $P(\epsilon_z)$ of the z component of local electric field arising from environment, evaluated at the oxygen site of each water molecule, (b) $P(\mu_z^e)$ of 1MES and (c) $P(\mu_z^e)$ for $\Delta E_a^i < 7.8$ eV: ambient (—); SCW1 (•••); SCW2 (—•••—); SCW3 (—•—).

in Figure 3a. Regardless of density, $P(\epsilon_z)$ is located mainly on the positive ϵ_z axis, so that the vacuum $\tilde{X}^1A_1$ and $\tilde{A}^1B_1$ states of water are stabilized and destabilized in solution, respectively. This solvation-induced destabilization of the excited state is in line with blue shift in Figure 2. As expected, $P(\epsilon_z)$ shifts toward higher field strength—viz., water becomes more polar—with increasing d. The TAB/10D results for the static dielectric constant ϵ_0 are 3.3, 7.6, 14.3, and 105 for SCW1, SCW2, SCW3, and AW, respectively.[42] Because of thermal fluctuations, $P(\epsilon_z)$ is characterized by a broad distribution; its width increases with d at fixed T. Thus, for instance, despite its average value of $\sim$1.5 V/Å, ϵ_z can sometimes exceed 2.5 V/Å in AW. This would induce highly polarized excited states, which have an important consequence for the Urbach tail in AW (see below).

We turn to the dipole moment of 1MES associated with the first absorption band of Figure 2. The probability distributions $P(\mu_z^e)$ of its z component, μ_z^e, at different water densities are exhibited in Figure 3b. We notice that, at a given fixed density, the excited-state dipole moment varies markedly. This arises from the solvation-dependent dipole enhancement induced by a fluctuating local electric field (Figure 3a). The modulation of the excited-state electronic character through d is also striking. At the lowest density $d = 0.22$ g cm^{-3} we studied, the maximum of the dipole distribution is located around $\mu_z^e = -1.3$ D. Thus, the majority of water molecules in SCW1 retain, to a large extent, the vacuum $\tilde{A}^1B_1$ character in their first excited states. Nevertheless, a long tail of the distribution indicates that a sizable amount of water undergoes a significant dipole enhancement because of solvation fluctuations. As d increases, the dipole distribution shifts in the positive μ_z^e direction; its peak position is $\mu_z^e \approx -0.8$ D for $d = 0.44$ g cm^{-3}, 0.0 D for 0.66 g cm^{-3}, and 4.5 D for 1 g cm^{-3}. This is due to the increasing local electric field strength with d, which in turn enhances the induced dipole moment of the water excited states. In view of the two-state analysis above, this means that electronic mixing of $\tilde{A}^1B_1$ and $\tilde{C}^1B_1$ grows with d. The inspection of the state coefficients shows that the first excited states in AW are on the average nearly 60−40 mixing of $\tilde{A}^1B_1$ and $\tilde{C}^1B_1$, while the latter accounts for $\lesssim$5% % in SCW1.

It is interesting that, despite their nearly identical energy gap distribution (Figure 3a), AW and SCW3 are characterized by totally different $P(\mu_z^e)$ in Figure 3b. To pursue this a little further, μ_z^e associated with the red edge of the energy gap distribution, i.e., $\Delta E_a^i < 7.8$ eV, is compared in Figure 3c. Its main contribution arises from the highly polarized excited states with $\mu_z^e \approx 5$ D in AW, while it is from nearly unpolarized states with $\mu_z^e \approx -1.2$ D in SCW3. This means that the water molecules subject to an extremely strong local electric field ($\epsilon_z \gtrsim 2.4$ V/Å) yield the red edge in the former, whereas it is relatively weak field ($\epsilon_z \lesssim 0.2$ V/Å) that is responsible in the latter.

Before we proceed to the exciton delocalization effects, we make brief contact with the Urbach tail observed experimentally in condensed phases (see section I). We attribute the appearance of the tail in AW to the electronic transitions to highly polarized excited states present under an extremely polar solvation configuration (cf. Figure 3c). This proposal provides a simple explanation for the temperature dependence[3−6,8] of the tail at normal density $d = 1$ g cm^{-3}. As T increases, $P(\epsilon_z)$ becomes broader and thus ϵ_z responsible for the Urbach tail becomes stronger. This results in better stabilization of the corresponding excited states, which then shifts the tail to lower energies. Because the thermal fluctuations of ϵ_z are larger in liquid water than in ice, our theory also predicts that the Urbach tail is more extended in the former than in the latter, consonant with experiments. However, the situation changes dramatically with the reduction of density. For SCW3 with $d = 0.66$ g cm^{-3}, the excited states relevant for the tail (viz., $\Delta E_a^i < 7.8$ eV) are characterized by small dipoles in the *negative* z direction, in total contrast with the AW case. We would thus expect that, at fixed T, the electronic character of the excited states associated with the Urbach tail changes from highly to weakly polarized and from positive to negative μ_z^e as the density diminishes. It would also be possible that, at some intermediate density, the

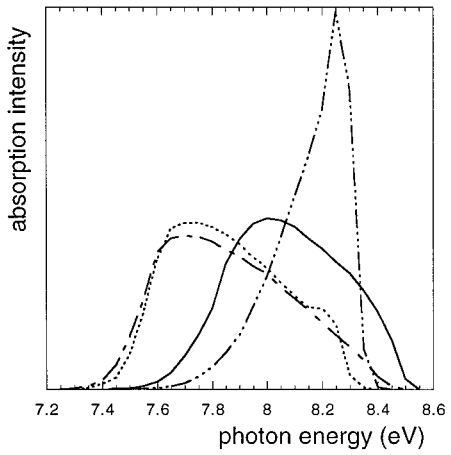

Figure 4. Lowest photoabsorption band of TAB/10D water with the inclusion of exciton delocalization via 1MCI: ambient (—); SCW1 (···). For comparison, the corresponding energy gap distributions in Figure 2 are repeated: ambient (—···—); SCW1 (···).

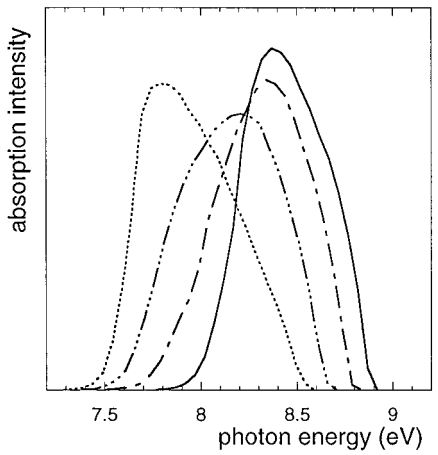

Figure 5. Rydbergization-corrected photoabsorption band of TAB/10D water with the inclusion of exciton delocalization: ambient (—); SCW1 (···); SCW2 (—···—); SCW3 (—·—).

tail would involve both highly polarized, positive and weakly polarized, negative μ_z^e. To test our proposal, we suggest an electroabsorption study[27] of water under differing thermodynamic conditions. To be specific, by the comparison of the absorption spectra in the presence and absence of an external electric field at various densities, one would be able to probe the excited-state dipole moment and polarizability and their variations with the photon energy. This would provide insight into the electronic character of the Urbach tail and its modulation with d.

We examine the influence of exciton delocalization on the first absorption band via the 1MCI method in eq 8. The results for AW and SCW1 are shown in Figure 4. We notice that the inclusion of 1MCI broadens the absorption spectrum and shifts it to low energies, compared to that obtained with the neglect of exciton delocalization. Also, as d increases, the 1MCI effects tend to grow because the number of neighboring water molecules available for exciton delocalization increases and their average distance from the central molecule decreases.[43] Thus, the ΔE_a^i distribution and 1MCI yield nearly the same spectral line shape for low-density SCW1. By contrast, the effects of exciton delocalization are very pronounced for high-density AW. For instance, the 1MCI prediction of its fwhm is about $\Delta_{solv} =$ 0.6 eV; this is a factor of 2 increase, compared to that obtained from the ΔE_a^i distribution. This broadening tends to reduce the character of the red tail of the absorption band, compared with Figure 2. Also the 1MCI result for blue shift in AW is about 0.3 eV smaller than that of the energy gap distribution. Thus, the former yields a blue shift of ~0.4−0.5 eV with respect to the vacuum absorption line. While this underestimates the observed value by ~0.3−0.4 eV, we stress that it correctly captures both the direction and order of magnitude of the spectral shift. We further note that the broader and more symmetric line shape of 1MCI agrees better with experiments[2−11] than the ΔE_a^i distribution in Figure 2.

It is worth mentioning here that the TAB/10D model also captures the photoabsorption properties of a water dimer reasonably well. Specifically, with the 1MCI method, we found that the lowest excitation of a dimer in the minimum-energy configuration[36] in the ground electronic state is blue-shifted by ~0.39 eV, compared to a monomer. This is in fair agreement with the ab initio calculations;[21−24] the MRCI and MCSCF methods, for example, yield spectral blue shift of 0.27[22] and 0.25 eV,[23] respectively.

C. Perspectives. Our results above paint the picture that solvation destabilization of $\tilde{A}^1B_1$, electronic mixing, and exciton delocalization play an important role in spectral line shape and blue shift of liquid water. To place this in perspective, we consider some of the aspects that are not properly reflected in our description. One is the Rydbergization[13] destabilization of the water excited states, mentioned above in section I. This is the conventional explanation invoked for spectral blue shift of water in the condensed phases.[14] In the TAB/10D model, because the Lennard-Jones interactions are assumed to be independent of electronic states, the Rydbergization is not accounted for in a strict sense.[44] This probably explains why the 1MCI underestimates the experimental blue shift by 0.3−0.4 eV for AW. To correct this, we approximately incorporate the Rydbergization effect into the absorption spectra by

$$\Delta E_{Ry} \propto n \int_0^\infty d\vec{r}\; g_{OO}(r)\, S(r) \tag{9}$$

where ΔE_{Ry} is the Rydbergization contribution to spectral shift, $g_{OO}(r)$ is the oxygen−oxygen radial distribution function, $S(r)$ is the electron overlap integral, and n is the water number density. We further approximate eq 9 as

$$\Delta E_{Ry} \approx R n \int_0^{r^*} d\vec{r}\; g_{OO}(r) \tag{10}$$

where r^* is an effective cutoff distance to model $S(r)$ and R is a proportionality constant. We choose $r^* = 3.5$ Å and $R =$ 0.07 eV assuming that $\Delta E_{Ry} \approx 0.35$ eV under an ambient condition. This yields $\Delta E_{Ry} \approx 0.09$, 0.16, 0.24, and 0.37 eV for SCW1, SCW2, SCW3, and AW, respectively.[45] The Rydbergization-corrected photoabsorption spectra—i.e., the 1MCI results of Figure 4 shifted by ΔE_{Ry}—under different thermodynamic conditions are shown in Figure 5. Except for the line width correction due to intramolecular dynamics (eq 11), the results there are the best predictions of the TAB/10D model within the 1MCI scheme. We notice that there is a close correlation—though nonlinear—between the average water density and spectral blue shift in the liquid and supercritical phases.[46] Because of the lack of experiments in the supercritical phase, comparison with measurements is not possible. It will thus be interesting to see if the results in Figure 5 are borne out as photoabsorption data for supercritical water become available in the future.

Another feature not included in our study is the line-broadening contribution from intramolecular dynamics. As

mentioned above, $\Delta_{vac} = 0$ in the TAB/10D description because of its rigid geometry, whereas $\Delta_{vac} \approx 1$ eV experimentally.[12] If we take account of the intramolecular contribution via

$$\Delta_{tot}^{\ 2} = \Delta_{solv}^{\ 2} + \Delta_{vac}^{\ 2} \tag{11}$$

the total fwhm in AW becomes $\Delta_{tot} \approx 1.2$ eV at the 1MCI level with $\Delta_{solv} = 0.6$ eV and $\Delta_{vac} = 1$ eV. This further improves the agreement with the experimental line shape for AW. On a related issue, only the solvation and exciton delocalization effects are reflected in our Δ_{solv} calculation. The inclusion of other electronic relaxation effects and thermal fluctuations of Rydbergization destabilization not considered here would also increase Δ_{solv} and thus Δ_{tot}.

While the TAB/10D model yields a red tail, it is not as extensive as in measurements. We believe that this is due to the underestimation of the excited-state dipole moments of AW in the presence of an extremely high local electric field. As pointed out above (Figure 1), because of the neglect of the highly excited states, the TAB description would underestimate the induced dipole moment of the low-lying excited states and thus their solvation stabilization, especially in the strong electric field regime. This would overestimate the electronic transition energies to highly polarized excited states that are mainly responsible for the Urbach tail. We would thus expect that the actual tail would be extended more toward longer wavelengths than predicted here. In principle, this situation could be improved considerably in the simulations within the TAB framework by introducing additional excited states which couple to $\tilde{A}^1B_1^{\epsilon}$ and $\tilde{C}^1B_1^{\epsilon}$. Also an excited-state partial charge transfer between water molecules[1a] not included in our description could further enhance the Urbach tail.

Finally, we briefly consider an implication of solvation-induced mixing of the excited electronic states on multiphoton ionization of water. The ground-state electronic configuration of water is $(1a_1)^2(2a_1)^2(1b_2)^2(3a_1)^2(1b_1)^2$, where the nonbonding $1b_1$ is essentially a $2p_x$ AO of oxygen. The $\tilde{A}^1B_1$ and $\tilde{C}^1B_1$ excited states, on the other hand, have strong $1b_1 \rightarrow 3sa_1$ and $1b_1 \rightarrow 3pa_1$ Rydberg character, respectively. Thus, we drastically simplify our description to treat $\tilde{X}^1A_1 \rightarrow \tilde{A}^1B_1$ and $\tilde{X}^1A_1 \rightarrow \tilde{C}^1B_1$ as mainly $p_x \rightarrow s$ and $p_x \rightarrow p_z$ transitions of oxygen AOs, respectively. Then, within the electric dipole framework, $\tilde{X}^1A_1 \rightarrow \tilde{A}^1B_1$would be three-photon-allowed because of the $p \rightarrow s$ character, while $\tilde{X}^1A_1 \rightarrow \tilde{C}^1B_1$would be two-photon-allowed because of $p \rightarrow p$.[47] This would mean that two-photon and three-photon excitations would populate preferentially the $\tilde{C}^1B_1$ ($3pa_1$) and $\tilde{A}^1B_1$ ($3sa_1$) components of the solution-phase first excited state, respectively. Because $3pa_1$ is much more diffuse than $3sa_1$, we would expect from the uncertainty principle that typical momentum and kinetic energy of electrons ejected from the former (and thus from $\tilde{C}^1B_1$) in the ionization would be lower than those from the latter (and thus from $\tilde{A}^1B_1$). As a result, the electrons produced via two-photon excitations would travel a shorter distance in the medium (before they become solvated) than those via three-photon absorptions. And, the ensuing geminate recombinations would be faster in the two-photon ionization than in the three-photon process. Another potentially important factor would be the correlation between water structure and electron solvation. The angular distribution of the electrons ejected from $3pa_1$ would be anisotropic because of its p_z nature, whereas $3sa_1$ would yield an isotropic distribution. Because electron solvation occurs very rapidly (its time scale, $\sim$1 ps,[48,49] is comparable to the water structural relaxation time[50,51]), the electrons resulting from anisotropic $3pa_1$ would probably see different water structure than those from isotropic $3sa_1$ during their initial localization into preexisting traps. This could also contribute to the difference in electron-cation distance distributions between the two- and three-photon excitations. Therefore, it would be of considerable interest to make a detailed comparison of recombination kinetics of two- and three-photon ionizations of water in the low irradiance limit where a 3+1 process is not accessible.[25,26]

V. Concluding Remarks

We have examined the electronic absorption spectra of water under ambient and supercritical conditions via the 1MCI method. By employing the TAB/10D model,[20a,b,36] solvation-induced electronic structure variations were explicitly accounted for in the simulations. The Rydbergization effect[14] was incorporated approximately via the oxygen−oxygen radial distribution at short separations. The first absorption band was found to be broadened and blue-shifted in liquid, compared to that in vacuum. The broadening arises from the inhomogeneous distribution of solvation environments, while the blue-shift is due to the solvation and Rydbergization destabilizations of the excited states.

The TAB/10D description yields a tail on the red edge of the absorption spectrum, although it is not as extensive as that in measurements. We found that thermal fluctuations of the local electric field and accompanying solvation-dependent electronic mixing of the vacuum $\tilde{A}^1B_1$ and $\tilde{C}^1B_1$ states are of primary importance to the appearance of the tail. To be specific, highly polarized excited states of water, existing under extremely polar solvation environments, are responsible for the tail in AW. By contrast, in low-density SCW, it arises from the relatively unpolarized excited states in the presence of weakly polar environments. To test this notion, we have proposed an electroabsorption study of water.

It would be worthwhile in the future to extend the TAB/10D description in more realistic directions. The direct incorporation of the Rydbergization destabilization into the simulations can be achieved by introducing state-dependent Lennard-Jones potentials. This will provide a great improvement over the approximate correction via eq 10, employed in the current study. Also polarizability enhancement for the excited states is needed to accurately describe the Urbach tail. This, together with the direct incorporation of Rydbergization, will further clarify the excited-state electronic structure variation with thermodynamic conditions and shed light on, e.g., the photoabsorption behavior of ice. Another important direction is the inclusion of intramolecular dynamics using flexible geometry. Finally, account of intermolecular partial charge transfer for both the ground and excited states of water would be a very desirable but challenging extension.

Acknowledgment. We would like to thank Dr. David Bartels for helpful discussions on multiphoton ionization of water. We acknowledge the donors of the Petroleum Research Fund, administered by the ACS, for partial support of this research. This work was also supported in part by NSF Grant CHE-9708575.

References and Notes

(1) For reviews, see: (a) Sander, M. U.; Luther, K.; Troe, J. *J. Phys. Chem.* **1993**, *97*, 953. (b) Bernas, A.; Ferradini, C.; Jay-Gerin, J.-P. *Chem. Phys.* **1997**, *222*, 151.

(2) Stevenson, D. P. *J. Phys. Chem.* **1965**, *69*, 2145.

(3) (a) Onaka, R.; Takahashi, T. *J. Phys. Soc. Jpn.* **1968**, *24*, 548. (b) Shibaguchi, T.; Onaka, R. *J. Phys. Soc. Jpn.* **1977**, *42*, 152.

(4) Verrall, R. E.; Senior, W. A. *J. Chem. Phys.* **1969**, *50*, 2746.
(5) Painter, L. R.; Birkhoff, R. D.; Arakawa, E. T. *J. Chem. Phys.* **1969**, *51*, 243. Kerr, G. D.; Hamm, R. N.; Williams, M. W.; Birkhoff, R. D.; Painter, L. R. *Phys. Rev. A* **1972**, *5*, 2523. Heller, J. M., Jr.; Hamm, R. N.; Birkhoff, R. D.; Painter, L. R. *J. Chem. Phys.* **1974**, *60*, 3483.
(6) Ghormley, J. A.; Hochanadel, C. J. *J. Phys. Chem.* **1971**, *75*, 40.
(7) Popova, S. I.; Alperovich, L. I.; Zolotarev, V. M. *Opt. Spectrosc.* **1972**, *32*, 288.
(8) Williams, F.; Varma, S. P.; Hillenius, S. *J. Chem. Phys.* **1976**, *64*, 1549.
(9) Quickenden, T. I.; Irvin, J. A. *J. Chem. Phys.* **1980**, *72*, 4416.
(10) Hayashi, H.; Watanabe, N.; Udagawa, Y.; Kao, C.-C. *J. Chem. Phys.* **1998**, *108*, 823.
(11) For earlier works, see references cited in ref 9.
(12) For experiments on water vapor, see: Chan, W. F.; Cooper, G.; Brion, C. E. *Chem. Phys.* **1993**, *178*, 387 and references therein.
(13) Mulliken, R. S. *Acc. Chem. Res.* **1976**, *9*, 7; *Chem. Phys. Lett.* **1977**, *46*, 197.
(14) Han, P.; Bartels, D. M. *J. Phys. Chem.* **1990**, *94*, 5824.
(15) Chergui, M.; Schwentner, M. *Chem. Phys. Lett.* **1994**, *219*, 237. Chergui, M.; Schwentner, M.; Stepanenko, V. *Chem. Phys.* **1994**, *187*, 153.
(16) Klein, S.; Kochanski, E.; Strich, A.; Sadlej, A. J. *Theor. Chim. Acta* **1996**, *94*, 75.
(17) Laasonen, K.; Sprik, M.; Parrinello, M.; Car, R. *J. Chem. Phys.* **1993**, *99*, 9080.
(18) Borgis, D.; Staib, A. *Chem. Phys. Lett.* **1995**, *238*, 187.
(19) Bursulaya, B. D.; Kim, H. J. *J. Chem. Phys.* **1998**, *108*, 3277.
(20) (a) Bursulaya, B. D.; Jeon, J.; Zichi, D. A.; Kim, H. J. *J. Chem. Phys.* **1998**, *108*, 3286. (b) Kim, H. J.; Bursulaya, B. D.; Jeon, J.; Zichi, D. A. *Proc. SPIE* **1998**, *3273*, 90. (c) *ACS Symp. Ser.* **1998**, *712*, 172.
(21) van Hemert, M.; van der Avoird, A. *J. Chem. Phys.* **1979**, *71*, 5310.
(22) Sosa, R. M.; Gardiol, P.; Ventura, O. N. *J. Mol. Struct.* **1993**, *297*, 337.
(23) Zvereva, N. A.; Ippolitov, I. I. *Proc. SPIE* **1997**, *3090*, 88.
(24) Harvey, J. N.; Jung, J. O.; Gerber, R. B. *J. Chem. Phys.* **1998**, *109*, 8747.
(25) Crowell, R. A.; Bartels, D. M. *J. Phys. Chem.* **1996**, *100*, 17940.
(26) Crowell, R. A.; Qian, J. *Irradiance and Isotope Effects for the 3 eV Multiphoton Ionization of Liquid Water*, unpublished.
(27) See, for example: Liptay, W. In *Modern Quantum Chemistry Part III: Action of Light and Organic Crystals*; Sinanoğlu, O., Ed.; Academic: New York, 1965; p 45. Bublitz, G. U.; Boxer, S. G. *Annu. Rev. Phys. Chem.* **1997**, *48*, 213.
(28) Even though the dipole approximation is employed throughout section II for convenience, the extended charge distributions are used in the actual simulations [see section IVA below].
(29) Szabo, A.; Ostlund, N. S. *Modern Quantum Chemistry*; McGraw-Hill: New York, 1982.
(30) Dunning, T. H., Jr. *J. Chem. Phys.* **1989**, *90*, 1007. Kendall, R. A.; Dunning, T. H., Jr.; Harrison, R. J. *J. Chem. Phys.* **1992**, *96*, 6769.
(31) Dunning, T. H., Jr.; Hay, P. J. In *Methods of Electronic Structure Theory*; Schaefer, H. F., III, Ed.; Plenum: New York, 1977; Vol. 3.
(32) Basis sets were obtained from the Extensible Computational Chemistry Environment Basis Set Database, Version 1.0, as developed and distributed by the Molecular Science Computing Facility, Environmental and Molecular Sciences Laboratory which is part of the Pacific Northwest Laboratory, P.O. Box 999, Richland, WA 99352, and funded by the U.S. Department of Energy.
(33) Schmidt, M. W.; Baldridge, K. K.; Boatz, J. A.; Elbert, S. T.; Gordon, M. S.; Jensen, J. H.; Koseki, S.; Matsunaga, N.; Nguyen, K. A.; Su, S. J.; Windus, T. L.; Dupuis, M.; Montgomery, J. A. *J. Comput. Chem.* **1993**, *14*, 1347.
(34) Berendsen, H. J. C.; Gigera, J. R.; Straatsma, T. P. *J. Phys. Chem.* **1987**, *91*, 6269.
(35) Among the vacuum energy eigenstates in Table 1, only $\tilde{C}^1B_1$ becomes coupled to $\tilde{A}^1B_1$ in the presence of ϵ_{ext} parallel to the *z* axis.
(36) Bursulaya, B. D.; Kim, H. J. *J. Chem. Phys.* **1999**, *110*, 9646.
(37) Nosé, S. *J. Chem. Phys.* **1984**, *81*, 511.
(38) Adams, D. J. *Chem. Phys. Lett.* **1979**, *62*, 329.
(39) Ryckaert, J.-P.; Ciccotti, G.; Berendsen, H. J. C. *J. Comput. Phys.* **1977**, *23*, 327.
(40) Verlet, L. *Phys. Rev.* **1967**, *159*, 98.
(41) Heyes, D. M. *J. Chem. Phys.* **1982**, *74*, 1924.
(42) The ϵ_0 values for AW and SCW3 are somewhat different from those reported in ref 36 due to differences in MD statistics. The current ϵ_0 estimations are based on a 1 ns trajectory in AW and a 500 ps trajectory in SCW3. Ensemble averages of other quantities in AW are computed with a 500 ps trajectory.
(43) The coupling elements in the 1MCI matrix (eq 8) are inversely propotional to the third power of the intermolecular separation.
(44) (a) We believe that the Rydbergization effect is reflected, to some degree, in the TAB/10D parametrization through the reduction of excited-state dipole moments, compared with the ab initio results. (b) The Rydbergization effect can be, in principle, incorporated explicitly into the simulations by the state-dependent Lennard-Jones interactions, so that the repulsion increases as water becomes more highly excited.
(45) The ΔE_{Ry} results remain essentially unchanged with a larger cutoff $r^* = 4.5$ Å (and properly scaled R).
(46) This trend could break down very close to the critical point because blue shift would be considerably influenced by local density augmentation.
(47) For real water, the $\tilde{X}^1A_1 \rightarrow \tilde{A}^1B_1$ and $\tilde{X}^1A_1 \rightarrow \tilde{C}^1B_1$ transitions are both two-photon- and three-photon-allowed because the excited MOs are linear combinations of many different AOs of oxygen and hydrogen.
(48) Migus, A.; Gauduel, Y.; Martin, J. L.; Antonetti, A. *Phys. Rev. Lett.* **1987**, *58*, 1559.
(49) Long, F. H.; Lu, H.; Eisenthal, K. B. *Phys. Rev. Lett.* **1990**, *64*, 1469.
(50) Litovitz, T. A.; Davis, C. M. In *Physical Acoustics*, Mason, W. P., Ed.; Academic: New York, 1965; Vol. IIA. Davis, C. M.; Jarzynski, J. In *Water: A Comprehensive Treatise*; Franks, F., Ed.; Plenum: New York, 1972; Vol. 1.
(51) Bursulaya, B. D.; Kim, H. J. *J. Chem. Phys.* **1998**, *109*, 4911.